SCIENTIFIC REPORTS

OPEN

Environment-insensitive and gate-controllable photocurrent enabled by bandgap engineering of MoS_2 junctions

Received: 25 October 2016
Accepted: 14 February 2017
Published: 21 March 2017

Fu-Yu Shih[1,2], Yueh-Chun Wu[2,†], Yi-Siang Shih[1], Ming-Chiuan Shih[3], Tsuei-Shin Wu[1,2], Po-Hsun Ho[4], Chun-Wei Chen[4], Yang-Fang Chen[1], Ya-Ping Chiu[1,5] & Wei-Hua Wang[2]

Two-dimensional (2D) materials are composed of atomically thin crystals with an enormous surface-to-volume ratio, and their physical properties can be easily subjected to the change of the chemical environment. Encapsulation with other layered materials, such as hexagonal boron nitride, is a common practice; however, this approach often requires inextricable fabrication processes. Alternatively, it is intriguing to explore methods to control transport properties in the circumstance of no encapsulated layer. This is very challenging because of the ubiquitous presence of adsorbents, which can lead to charged-impurity scattering sites, charge traps, and recombination centers. Here, we show that the short-circuit photocurrent originated from the built-in electric field at the MoS_2 junction is surprisingly insensitive to the gaseous environment over the range from a vacuum of 1×10^{-6} Torr to ambient condition. The environmental insensitivity of the short-circuit photocurrent is attributed to the characteristic of the diffusion current that is associated with the gradient of carrier density. Conversely, the photocurrent with bias exhibits typical persistent photoconductivity and greatly depends on the gaseous environment. The observation of environment-insensitive short-circuit photocurrent demonstrates an alternative method to design device structure for 2D-material-based optoelectronic applications.

Generally, two-dimensional (2D) materials, composed of atomically thin crystals, exhibit an enormous surface-to-volume ratio, and the physical properties of 2D materials, including electrical, optical, and mechanical properties, are easily subjected to the change of the chemical environment[1–6]. Regarding the electrical property, the carrier transport in 2D materials is very sensitive to the presence of extrinsic adsorbents, which typically cause charged-impurity scattering, charge trapping, and recombination centers[7–11], leading to degradation of the transport characteristics[12–14]. Although various encapsulation methods have been developed[15–19], it is intriguing to explore methods to control the transport properties in the circumstance of no encapsulated layer. Here, we demonstrated that the short-circuit photocurrent enabled by the built-in electric field at the MoS_2 junction is surprisingly insensitive to the gaseous environment, which is very uncommon in the photoresponse of thin transition-metal dichalcogenides (TMDCs). We exploit the unique property of 2D TMDCs, in which the electronic band structures are associated with the number of the layered materials[20,21], to create a junction structure. For molybdenum disulfide (MoS_2), the transition changes from direct bandgap (1.9 eV) in monolayer MoS_2 to indirect bandgap (1.3 eV) in bulk MoS_2[22–24]. This layer-dependent electronic structure therefore offers a distinct approach for designing the MoS_2 junction based on homogeneous material of the TMDCs[25–28].

In this work, we fabricated atomic thin MoS_2 junction phototransistors with different MoS_2 layers and studied their photoresponse behavior at different source-drain bias and gaseous environment. The difference of band gap in different thickness of few layer MoS_2 was utilized to create a built-in electric field. Interestingly, we observed

[1]Department of Physics, National Taiwan University, Taipei 106, Taiwan. [2]Institute of Atomic and Molecular Sciences, Academia Sinica, Taipei 106, Taiwan. [3]Department of Physics, National Sun Yat-sen University, Kaohsiung, Taiwan. [4]Department of Materials Science and Engineering, National Taiwan University, Taipei 106, Taiwan. [5]Institute of Physics, Academia Sinica, Taipei 115, Taiwan. [†]Present address: Department of Physics, University of Massachusetts, Amherst, Massachusetts 01003, United States. Correspondence and requests for materials should be addressed to W.-H.W. (email: wwang@sinica.edu.tw)

that the short-circuit photocurrent due to the photovoltaic (PV) effect[29] is insensitive to the gaseous environment over the range from a vacuum of 1×10^{-6} Torr to ambient condition. This environmental insensitivity can be well ascribed to the unique characteristic of diffusion current that is associated with the carrier density gradient. Conversely, the photocurrent under bias exhibits persistent photoconductivity (PPC) and highly depends on the gaseous environment. The scanning tunneling microscopy and spectroscopy (STM and STS) measurements reveal the energy profile at the MoS_2 junction, confirming the presence of the band offset. Moreover, we show that the MoS_2 junction phototransistors exhibit gate-voltage tunable open-circuit voltage and short-circuit photocurrent, demonstrating the capability for regulating the current-voltage characteristics of the MoS_2 junction via electric field effect.

The details of sample fabrication processes are described in the Supporting Information S1. In brief, MoS_2 junctions with different layers were prepared by mechanically exfoliating MoS_2 crystals onto SiO_2(300 nm)/Si substrates. We then identify MoS_2 flakes with different numbers of layers using optical microscopy. The thicknesses of the flakes of MoS_2 were characterized using atomic force microscopy and Raman spectroscopy (Supporting Information S2). We then employ a resist-free approach to define the electrical contact to the MoS_2 junction to avoid the resist residue which may cause extra carrier scattering. We then deposited Au (50 nm) for the electrical contacts by e-beam evaporation at a base pressure of 1×10^{-7} Torr.

Results and Discussion

We studied the photoresponse behavior of the MoS_2 junction devices to investigate the PV effect due to the built-in electric field. Figure 1a,b show a schematic of the device structure of MoS_2 1L-3L junction with Au electrodes and an optical microscopy image of a typical MoS_2 junction device (sample A), respectively. For sample A, the total channel length is 5 μm, and the thin and thick regions of the MoS_2 junctions are 0.7 and 1.9 nm, respectively. We performed the photocurrent measurement with a photoexcitation (532 nm, 20 kW/cm^2) focused at the MoS_2 junction interface at $V_G = 60$ V. Figure 1c compares the photocurrent at $V_{SD} = 0$ mV and $V_{SD} = 50$ mV, in which we readily found drastically different photoresponse between zero and small V_{SD}. For $V_{SD} = 50$ mV, the photocurrent exhibits a PPC which is the photocurrent that persists after the photoexcitation is terminated. For a disordered system, it is common to use the stretched exponential decay to describe the PPC relaxation[30–32]. Here, we can analyze the photocurrent relaxation by a single stretched exponential decay[33]

$$I(t) = I_0 \exp[-(t/\tau)^{\beta}] \quad (1)$$

where τ is the decay time, and β is the exponent ($0 < \beta < 1$), yielding $\tau = 90$ s for $V_{SD} = 50$ mV. The decay time is comparable to the previous study[30], suggesting that the observed PPC effect in the MoS_2 sample is originated from random localized potential fluctuation[30–32]. In contrast, the short-circuit photocurrent (I_{SC}) at zero bias is simply due to the PV effect driven by the built-in electric field, which exhibits a fast switching behavior and returns to the dark current level rapidly after illumination is terminated. The photocurrent relaxation can be fitted by a normal exponential decay ($\beta = 1$ in Equation 1)[34–36]. The value of τ is extracted to be approximately 60 ms, which are smaller than that under bias ($V_{SD} = 50$ mV) by 3 orders of magnitude (Supporting information 3).

The drastic difference between photoresponse with and without applying V_{SD} is intriguing and can be attributed to the difference in the carrier transport mechanism[37]. Here, we mainly focus on the slow-changing photocurrent that distinguishes the two scenarios. The current in the channel can be expressed as $J_n = J_n(drift) + J_n(diffusion) = e\mu_n nE - eD_n dn/dx$. The carrier density is varied temporally due to the trapping and de-trapping process in the illumination and dark condition, respectively. Because the photoconductivity (PC) is determined by the drift current, which is proportional to the carrier density, the PC is greatly affected by the presence of the charge traps. In contrast, when no bias voltage is applied, I_{SC} is induced by the built-in electric field at the junction and then driven by the diffusion current in the channel, which is proportional to the gradient of the carrier density dn/dx. Because dn/dx is related to the gradient of quasi-Fermi level dF_n/dx but not the carrier density, it is much less sensitive to the trapping/de-trapping processes. Therefore, I_{SC} exhibits a much faster photoresponse and the PPC effect can be greatly suppressed when the photocurrent is dominated by the short-circuit current.

Interestingly, the short-circuit photocurrent is virtually insensitive to the variation of the gaseous conditions over a range from a vacuum of 1×10^{-6} Torr to ambient condition. Here, we present this unique characteristic by showing the V_{SD} dependent photocurrent (I_{ph}) in different gaseous environment. Figure 2a compares I_{ph} of a 1L-3L MoS_2 junction (sample B) at $V_{SD} = 0$ mV among vacuum, N_2 (1 atm), and ambient condition, revealing that the magnitude of the I_{SC} (ΔI_{SC}) is insensitive to the environment. We note that in all 5 1L-3L samples that we measured, the photoresponse behavior is comparable and therefore the data shown here is representative. Under very different pressure and chemical substances, ΔI_{SC} exhibits essentially the same value of approximately 140 pA. Moreover, the decay time (τ) values for these different conditions are also similar, as described in detail in Supporting information S3. In contrast, the photocurrent of sample B under bias critically depends on the environmental conditions. Figure 2b shows I_{ph} at $V_{SD} = 5$ mV under vacuum, N_2, and ambient conditions, indicating the changes in photocurrent (ΔI_{PC}) for these three conditions are 263, 133, and 41 pA, respectively. Here we note that while ΔI_{SC} is only governed by the built-in electric field, ΔI_{PC} is referred to PC that is determined by both built-in field and external bias. Moreover, the sample exhibits larger τ under vacuum (90 sec) as compared to the τ under N_2 (16 sec) and ambient (8 sec) conditions. This dependence of I_{ph} on the chemical environment is typical for the 2D-material devices. The extracted parameters of mobility, threshold voltage, ΔI_{SC}, and ΔI_{PC} are listed in Table 1.

As previously discussed, I_{SC} is driven by the diffusion current that is related to the gradient of carrier density. This gradient is associated with the condition of illumination, but is negligibly affected by the trapping process and the presence of adsorbents. Consequently, both the magnitude and the response time of I_{SC} are very

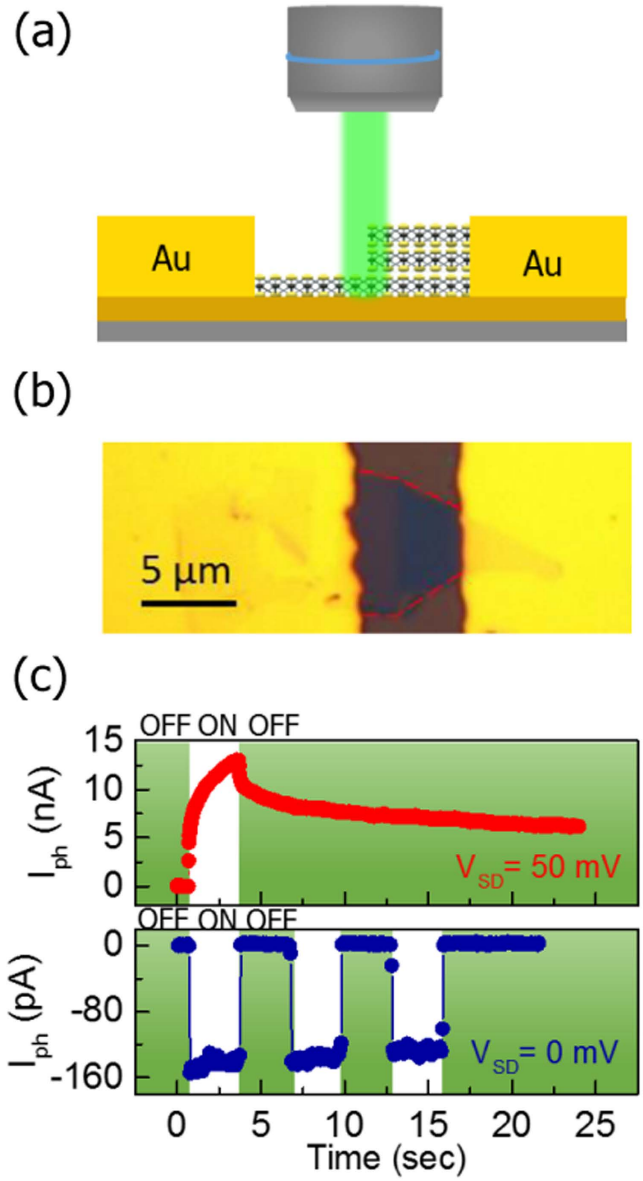

Figure 1. The structure and the photoresponse behaviors of the MoS_2 junctions. (**a**) A schematic diagram of a 1L-3L MoS_2 junction transistor with the excitation beam focused on the MoS_2 junction. (**b**) Optical image of a MoS_2 junction transistor. The edge of the MoS_2 junction is outlined by red lines. (**c**) Time-resolved photoresponse behaviors of the MoS_2 junction transistor (sample A) under $V_{SD} = 50$ mV (red curve) and $V_{SD} = 0$ mV (blue curve) at $V_G = 60$ V.

insensitive to the gaseous environment, despite the pressure and the chemical composition being very different. We note that this insensitivity of the photocurrent in MoS_2 junctions is very uncommon in 2D-material-based devices, considering the ultrahigh surface-to-volume ratio that leads to a large area being exposed to absorbents. Conversely, when bias voltage is applied, the carriers could be trapped or released during illumination and dark conditions, leading to the charging and the PPC effect, as seen in Fig. 2b.

To further investigate the observed PV effect due to the built-in electric field, we present the V_{SD} dependence of the photocurrent. Figure 3a shows a schematic diagram of energy band alignment and photoinduced carrier dynamics in the MoS_2 heterojunction. Type-I band alignment is implied based on the STS results shown in Fig. 4d,e. At zero bias, the photocurrent is mainly driven by the built-in field under illumination (Supporting Information S4), whereas both the built-in and the external field co-exist when bias voltage is applied. It is noted that only the electron conduction is considered here because all the MoS_2 junction samples exhibit n-type semiconducting behavior (Supporting Information S1). We considered the photocurrent under two polarity of bias (the detailed calculation of ΔI_{SC} and ΔI_{PC} are described in Supporting Information S5). The fast photoresponse of the photocurrent is negative, regardless of the polarity of bias, indicating that I_{SC} is induced by the built-in electric field. We then compared the photocurrent of sample B corresponding to the PV and the charging/discharging effect as a function of V_{SD} in small bias regime, as shown Fig. 3b. ΔI_{SC} is found to be

	Vacuum	N_2	Ambient
Mobility	0.5 cm^2/Vs	0.14 cm^2/Vs	0.09 cm^2/Vs
Threshold voltage	5.5 V	20 V	25.5 V
ΔI_{SC}			
$V_{SD} = 0$ mV	−136 pA	−143 pA	−149 pA
ΔI_{PC}			
$V_{SD} = 5$ mV	263 pA	133 pA	41 pA

Table 1. The characteristics of the MoS_2 junction (sample B) under different gaseous conditions.

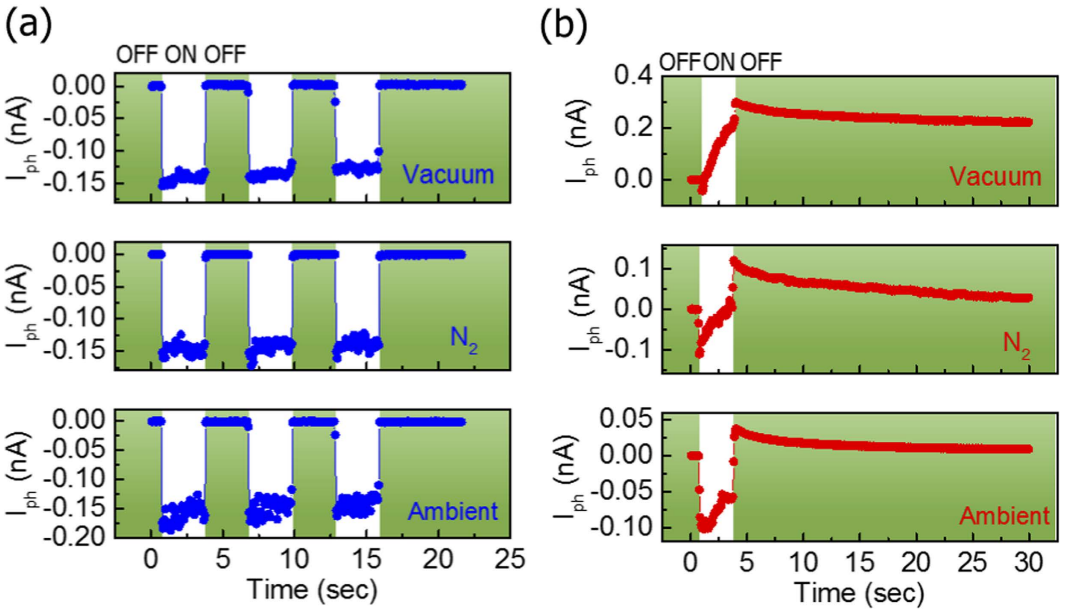

Figure 2. Time-resolved photoresponse of the MoS_2 junctions. The photocurrent behavior of the MoS_2 junction transistor (sample B) under different gaseous conditions at (**a**) $V_{SD} = 0$ mV and (**b**) $V_{SD} = 5$ mV. The short-circuit photoresponse is virtually insensitive to the variation of the gaseous conditions.

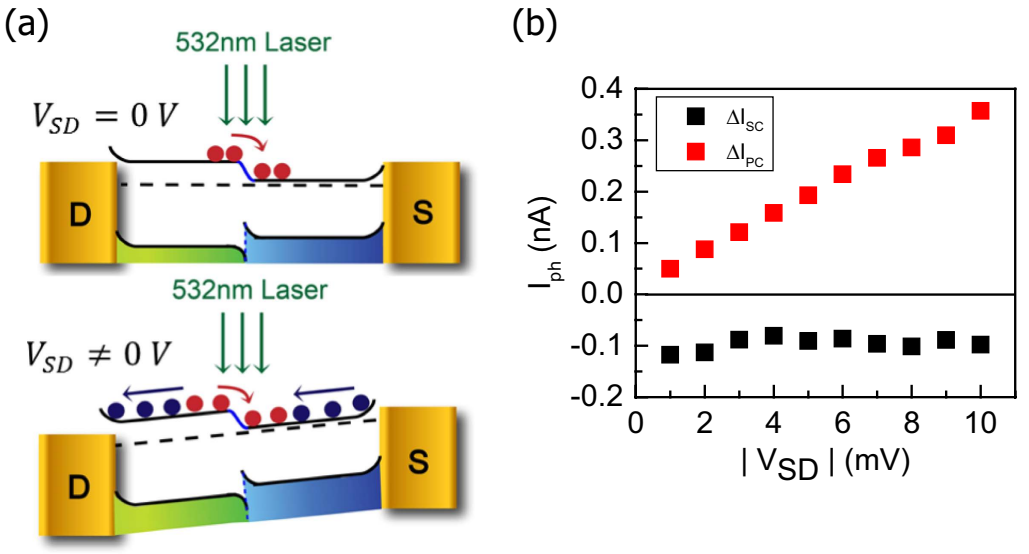

Figure 3. V_{SD}-dependent photoresponse of the MoS_2 junctions. (**a**) A schematic of the band structure of the MoS_2 junction transistor and photoinduced carrier transfer at $V_{SD} = 0$ V and $V_{SD} \neq 0$ V. (**b**) The photocurrent measurement of sample B corresponding to the photovoltaic effect (black squares) and the photoconductivity effect (red squares) as a function of V_{SD} at $V_G = 60$ V. The excitation power is 200 μW.

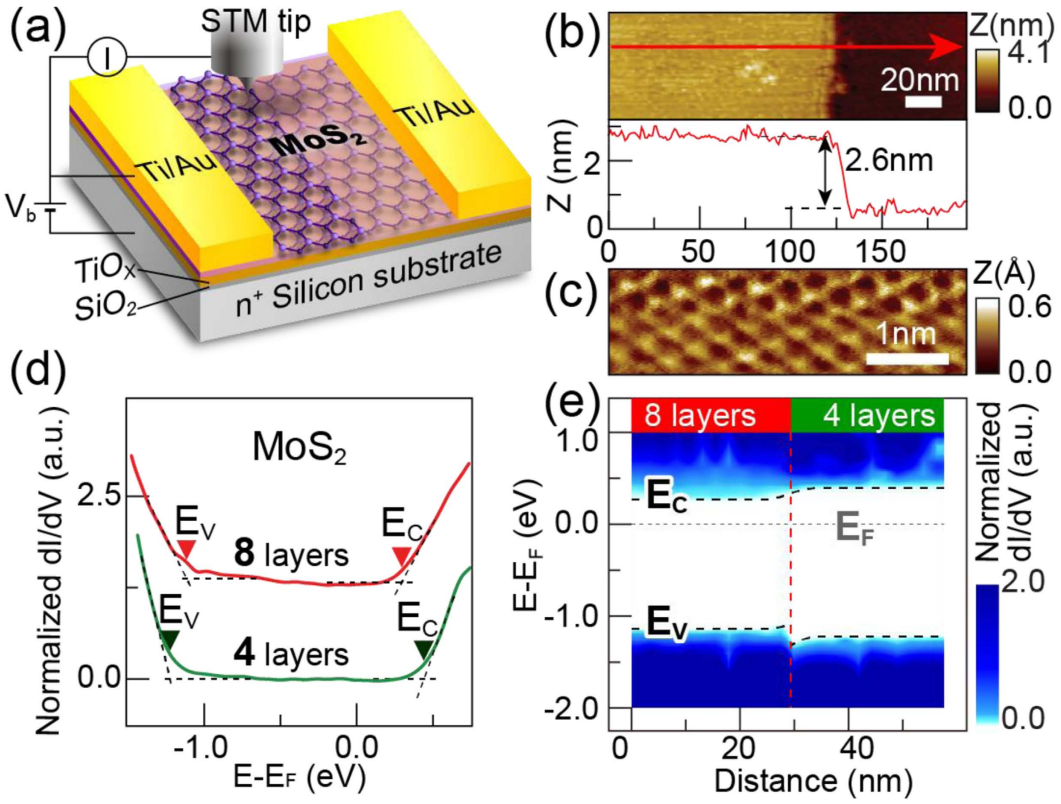

Figure 4. The STM/STS measurement of the MoS_2 junctions. (**a**) A schematic of the MoS_2 junction structure with different layer in the STM/STS measurement. (**b**) Top: STM topography image of the MoS_2 junction (sample C). Bottom: a cross-sectional topographic profile of the MoS_2 junction. (**c**) An STM image of sample C with atomic-scale resolution, which indicates a pristine MoS_2 surface. (**d**) Normalized dI/dV curves of 4 layer (green curve) and 8 layer (red curve) MoS_2. The profiles are offset for clarity. (**e**) Band alignment across the MoS_2 4- to 8-layer junction. Type-I band alignment at the MoS_2 junction was implied.

relatively independent of V_{SD}; this response is ascribed to the cancellation of the external field. In contrast, ΔI_{PC}, and thus the charging/discharging effect, increases linearly with V_{SD}; this response may be due to the phenomenon that the carriers are driven to the local potential minimum more efficiently with increasing bias.

Figure 4a shows a schematic of the experimental setup for the STM measurement on the MoS_2 junction transistors. Before MoS_2 exfoliation, we deposited a thin TiO_x film of 5 nm[38], which served as electron transfer dopant on MoS_2 flakes[39], resulting in the reduction of MoS_2 sheet resistance. The deposition of a TiO_x layer is therefore crucial for preventing of the STM tip from crashing during the measurement. Figure 4b shows a topography image of the MoS_2 junction device (sample C) at the junction, revealing the step with two flat terraces. The apparent step height is 2.6 nm, corresponding to 4 layers of MoS_2. Because the thinner MoS_2 is characterized by AFM as 4 layers, the studied MoS_2 sample is therefore a 4- to 8-layer junction. Figure 4c shows a high magnification topography image of MoS_2 that reveals crystalline structure, indicating a pristine MoS_2 surface.

To investigate the band alignment at the MoS_2 junction, the STS technique was utilized to measure the normalized dI/dV as a function of bias, which corresponds to the local density of state (LDOS). Figure 4d shows the bias dependence of dI/dV curve for the two MoS_2 terraces with different thicknesses. The onsets of the normalized dI/dV curves at positive and negative bias correspond to the conduction band edge (E_C) and the valance band edge (E_V), respectively (Supporting information S6). From the STS measurement, we deduce the following: the E_C and E_V in 8-layer MoS_2 are 0.29 eV and −1.12 eV, respectively; the E_C and E_V in 4-layer MoS_2 are 0.44 eV and −1.22 eV, respectively. By spatially mapping the normalized dI/dV curves, we plot the band alignment across the 4- to 8-layer junction, as shown in Fig. 4e. The deduced energy profile suggests that the band alignment of the MoS_2 junction is type I, as depicted in Fig. 3a.

Finally, we present the current-voltage characteristics at different V_G to analyze the field effect of the photocurrent in the MoS_2 junction devices. Figure 5a compares the $I_{SD} - V_{SD}$ curves of sample B in dark and under illumination with a 532 nm laser and 20 kW/cm^2 at $V_G = 60$ V. The $I_{SD} - V_{SD}$ curves exhibit a linear behavior, indicating that resistor behavior, rather than the rectifying effect, dominates the transport property of the junctions. The slope of the $I_{SD} - V_{SD}$ curves therefore approximates the conductance (G) of the device. Under illumination, G is enhanced by 40 times compared with G in dark; this enhancement is attributed to the generation of the photoinduced carriers. The open-circuit voltage (V_{OC}) and I_{SC} can be extracted as 60 μV and 0.12 nA, respectively. We note that the I_{SC} can be further enhanced by reducing the Schottky barrier height via contact engineering.

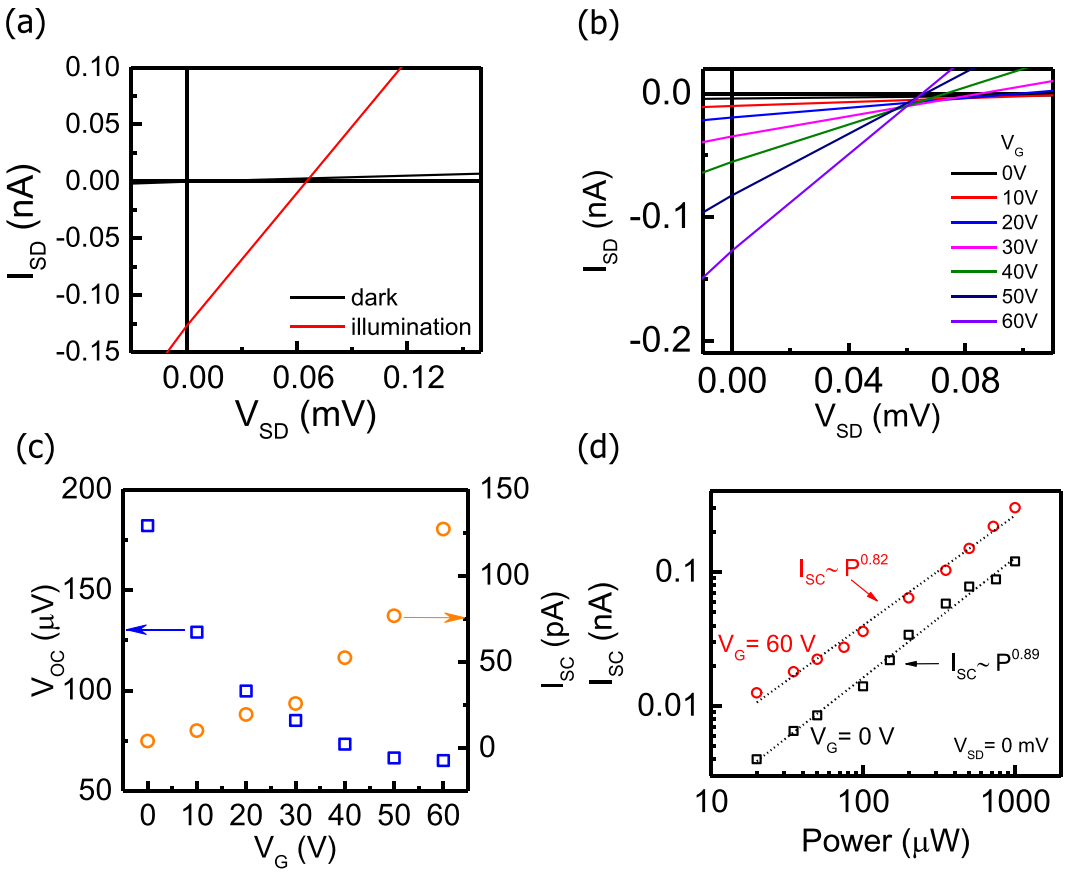

Figure 5. Field-effect-controlled short-circuit photocurrent of the MoS_2 junction transistors. (**a**) Output curves of the MoS_2 junction device (sample B) in dark (black curve) and under 532 nm excitation focused on the MoS_2 junction (red curve) at $V_G = 60$ V. (**b**) V_G dependence of the output curves under laser illumination ($P = 200\,\mu W$) at the MoS_2 junction. (**c**) Analysis of V_G dependence of V_{OC} and I_{SC} extracted from the output curves. (**d**) Excitation power dependence of I_{SC} at zero bias at $V_G = 0$ V (black squares) and $V_G = 60$ V (red circles). The dashed lines are fitting curves of power law $I_{SC} \propto P^{\alpha}$.

Because the Fermi level in thin materials can be effectively tuned by the external electric field, it is intriguing to study the field effect of the current-voltage characteristics. Indeed, we observed a V_G dependence of the $I_{SD} - V_{SD}$ curves under illumination, as shown in Fig. 5b, in which G increases with increasing V_G. To understand this field effect, we plot V_{OC} and I_{SC} as a function of V_G, as shown in Fig. 5c. I_{SC} is found to increase with increasing V_G, similar to the $I_{SD} - V_G$ curve (see Figure S1 of SI 1). This similarity is reasonable because I_{SC} depends on the collection probability of the photoinduced carriers, which is correlated to the diffusion current and G. Moreover, as V_G increases, the contact resistance may decrease due to Schottky barrier thinning[40], leading to higher I_{SC}. Conversely, the response of V_{OC} decreasing with increasing V_G can be attributed to the reduction of built-in electric field in the MoS_2 junction. Because monolayer MoS_2 is subjected to a stronger field effect compared with the few-layer MoS_2 due to the different density of states, the rising of Fermi level in monolayer MoS_2 is greater than that in few-layer MoS_2 as V_G increases, resulting in the reduction of the built-in electric field (see Fig. 3a) and thus V_{OC}.

We further present the excitation power dependence of I_{SC} at zero bias voltage (Fig. 5d) to examine the mechanism of the photocurrent generation[41]. We observe that I_{SC} follows a power law $I_{SC} \propto P^{\alpha}$, and the exponent α can be been extracted as 0.89 and 0.82 for $V_G = 0$ and 60 V, respectively. For the PC and the PV process, the photoinduced carrier density is directly proportional to the rate of absorbed photons; therefore, $\alpha = 1$[42]. However, because the PC is excluded here ($V_{SD} = 0$), the value of α therefore suggests that the PV is the dominant mechanism in the measured photocurrent. The deviation of the extracted α from unity may be attributed to electron-hole recombination at the MoS_2 junction and/or nonradiative recombination centers[43,44].

In conclusion, we demonstrated a unique environment-insensitive and gate-controllable short-circuit photocurrent in a MoS_2 junction with differences in the number of layer. The environmental insensitivity of the short-circuit photocurrent can be attributed to the characteristic of the diffusion current. Conversely, the photocurrent with bias exhibits the typical PPC that greatly depends on the amount of the extrinsic adsorbents. The STM/STS measurement confirms the quality of the MoS_2 junction samples and suggests the type-I band alignment of the junction. In addition to the effect of source-drain bias, the MoS_2 junction devices exhibit strong back-gate voltage dependence, indicating the feasibility to control the photocurrent via field effect. The

environment-insensitive photocurrent therefore shows an alternative method to design the device structure for TMDC-based electronic and optoelectronic applications.

Methods

Sample preparation. The sample with the 1L-3L MoS_2 junction was produced via mechanical exfoliation of MoS_2 layers from the bulk MoS_2 (SPI supplies) onto SiO_2 (300 nm)/Si substrates. Next, a resist-free technique with a shadow mask (TEM grids) was utilized to deposit electrical contacts. The advantage of the resist-free technique is the lack of resist residue on the MoS_2 surface resulting from the device fabrication process. We deposited Au (50 nm) as the electrical contacts using an electron-beam evaporator at a base pressure of 1.0×10^{-7} Torr. All of our MoS_2 junction devices were measured in a cryostat (Janis Research Company, ST-500) under vacuum condition of 1.0×10^{-6} Torr. We performed DC electrical measurement using a Keithley 237 sourcemeter and applied the back-gate voltage using a Keithley 2400 sourcemeter. We employed solid-state CW laser (Nd:YAG, 532 nm) as the light source in the Raman spectroscopy and photoresponse measurements. The incident light beam was focused by an objective (100×, NA 0.6) with a spot size of ~0.9 μm.

References

1. Geim, A. K. & Novoselov, K. S. The rise of graphene. *Nature materials* **6,** 183–191 (2007).
2. Schedin, F. *et al.* Detection of individual gas molecules adsorbed on graphene. *Nature materials* **6,** 652–655 (2007).
3. Varghese, S. S., Varghese, S. H., Swaminathan, S., Singh, K. K. & Mittal, V. Two-Dimensional Materials for Sensing: Graphene and Beyond. *Electronics* **4,** 651–687 (2015).
4. Tongay, S. *et al.* Broad-range modulation of light emission in two-dimensional semiconductors by molecular physisorption gating. *Nano letters* **13,** 2831–2836 (2013).
5. He, R. *et al.* Large physisorption strain in chemical vapor deposition of graphene on copper substrates. *Nano letters* **12,** 2408–2413 (2012).
6. Perkins, F. K. *et al.* Chemical vapor sensing with monolayer MoS2. *Nano letters* **13,** 668–673 (2013).
7. Ando, T. Screening effect and impurity scattering in monolayer graphene. *Journal of the Physical Society of Japan* **75,** 074716 (2006).
8. Hwang, E., Adam, S. & Sarma, S. D. Carrier transport in two-dimensional graphene layers. *Physical Review Letters* **98,** 186806 (2007).
9. Bolotin, K. I. *et al.* Ultrahigh electron mobility in suspended graphene. *Solid State Communications* **146,** 351–355 (2008).
10. Ma, N. & Jena, D. Charge scattering and mobility in atomically thin semiconductors. *Physical Review X* **4,** 011043 (2014).
11. Furchi, M. M., Polyushkin, D. K., Pospischil, A. & Mueller, T. Mechanisms of Photoconductivity in Atomically Thin MoS_2. *Nano Lett.* **14,** 6165–6170, doi: 10.1021/n1502339q (2014).
12. Chen, J.-H. *et al.* Charged-impurity scattering in graphene. *Nature Physics* **4,** 377–381 (2008).
13. Tan, Y.-W. *et al.* Measurement of scattering rate and minimum conductivity in graphene. *Physical review letters* **99,** 246803 (2007).
14. Chen, J.-H., Jang, C., Xiao, S., Ishigami, M. & Fuhrer, M. S. Intrinsic and extrinsic performance limits of graphene devices on SiO_2. *Nature nanotechnology* **3,** 206–209 (2008).
15. Jena, D. & Konar, A. Enhancement of carrier mobility in semiconductor nanostructures by dielectric engineering. *Physical review letters* **98,** 136805 (2007).
16. Kretinin, A. *et al.* Electronic properties of graphene encapsulated with different two-dimensional atomic crystals. *Nano letters* **14,** 3270–3276 (2014).
17. Ho, P.-H. *et al.* Self-encapsulated doping of n-type graphene transistors with extended air stability. *ACS nano* **6,** 6215–6221 (2012).
18. Lee, G.-H. *et al.* Highly Stable, Dual-Gated MoS2 Transistors Encapsulated by Hexagonal Boron Nitride with Gate-Controllable Contact, Resistance, and Threshold Voltage. *ACS nano* **9,** 7019–7026 (2015).
19. Li, L. *et al.* Quantum Hall effect in black phosphorus two-dimensional electron system. *Nature Nanotechnology* (2016).
20. Kuc, A., Zibouche, N. & Heine, T. Influence of quantum confinement on the electronic structure of the transition metal sulfide T S 2. *Physical Review B* **83,** 245213 (2011).
21. Yun, W. S., Han, S., Hong, S. C., Kim, I. G. & Lee, J. Thickness and strain effects on electronic structures of transition metal dichalcogenides: 2H-M X 2 semiconductors (M = Mo, W; X = S, Se, Te). *Physical Review B* **85,** 033305 (2012).
22. Mak, K. F., Lee, C., Hone, J., Shan, J. & Heinz, T. F. Atomically thin MoS_2: a new direct-gap semiconductor. *Physical Review Letters* **105,** 136805 (2010).
23. Splendiani, A. *et al.* Emerging photoluminescence in monolayer MoS2. *Nano letters* **10,** 1271–1275 (2010).
24. Cheiwchanchamnangij, T. & Lambrecht, W. R. Quasiparticle band structure calculation of monolayer, bilayer, and bulk MoS_2. *Physical Review B* **85,** 205302 (2012).
25. Howell, S. L. *et al.* Investigation of Band-Offsets at Monolayer–Multilayer MoS_2 Junctions by Scanning Photocurrent Microscopy. *Nano letters* **15,** 2278–2284 (2015).
26. Tosun, M. *et al.* MoS_2 Heterojunctions by Thickness Modulation. *Scientific reports* **5** (2015).
27. Baugher, B. W. H., Churchill, H. O. H., Yang, Y. F. & Jarillo-Herrero, P. Optoelectronic devices based on electrically tunable p-n diodes in a monolayer dichalcogenide. *Nat Nanotechnol* **9,** 262–267, doi: 10.1038/Nnano.2014.25 (2014).
28. Pospischil, A., Furchi, M. M. & Mueller, T. Solar-energy conversion and light emission in an atomic monolayer p-n diode. *Nat Nanotechnol* **9,** 257–261, doi: 10.1038/Nnano.2014.14 (2014).
29. Fontana, M. *et al.* Electron-hole transport and photovoltaic effect in gated MoS_2 Schottky junctions. *Sci Rep-Uk* **3,** doi:Artn 1634, doi: 10.1038/Srep01634 (2013).
30. Wu, Y. C. *et al.* Extrinsic Origin of Persistent Photoconductivity in Monolayer MoS_2 Field Effect Transistors. *Sci Rep* **5,** 11472, doi: 10.1038/srep11472 (2015).
31. Jiang, H. X. & Lin, J. Y. Percolation transition of persistent photoconductivity in II-VI mixed crystals. *Phys Rev Lett* **64,** 2547–2550, doi: 10.1103/PhysRevLett.64.2547 (1990).
32. Dissanayake, A. S., Huang, S. X., Jiang, H. X. & Lin, J. Y. Charge Storage and Persistent Photoconductivity in a Cds0.5se0.5 Semiconductor Alloy. *Phys Rev B* **44,** 13343–13348, doi: 10.1103/PhysRevB.44.13343 (1991).
33. Palmer, R. G., Stein, D. L., Abrahams, E. & Anderson, P. W. Models of Hierarchically Constrained Dynamics for Glassy Relaxation. *Phys. Rev. Lett.* **53,** 958–961 (1984).
34. Yin, Z. Y. *et al.* Single-Layer MoS_2 Phototransistors. *ACS Nano* **6,** 74–80, doi: 10.1021/Nn2024557 (2012).
35. Lee, H. S. *et al.* MoS_2 Nanosheet Phototransistors with Thickness-Modulated Optical Energy Gap. *Nano Lett.* **12,** 3695–3700, doi: 10.1021/Nl301485q (2012).
36. Chen, S. Y. *et al.* Biologically inspired graphene-chlorophyll phototransistors with high gain. *Carbon* **63,** 23–29, doi: 10.1016/j.carbon.2013.06.031 (2013).
37. Sze, S. M. & Ng, K. K. *Physics of semiconductor devices* (John wiley & sons, 2006).
38. Ho, P. H. *et al.* Precisely Controlled Ultrastrong Photoinduced Doping at Graphene–Heterostructures Assisted by Trap-State-Mediated Charge Transfer. *Advanced materials* **27,** 7809–7815 (2015).

39. Rai, A. *et al.* Air stable doping and intrinsic mobility enhancement in monolayer molybdenum disulfide by amorphous titanium suboxide encapsulation. *Nano letters* **15,** 4329–4336 (2015).
40. Li, S.-L. *et al.* Thickness Scaling Effect on Interfacial Barrier and Electrical Contact to Two-Dimensional MoS_2 Layers. *ACS Nano*, doi: 10.1021/nn506138y (2014).
41. Zhang, Y. *et al.* Photothermoelectric and photovoltaic effects both present in MoS_2. *Scientific reports* **5,** 7938, doi: 10.1038/srep07938 (2015).
42. Patil, V., Capone, A., Strauf, S. & Yang, E.-H. Improved photoresponse with enhanced photoelectric contribution in fully suspended graphene photodetectors. *Scientific reports* **3** (2013).
43. Zhang, W. *et al.* High-gain phototransistors based on a CVD MoS(2) monolayer. *Advanced materials* **25,** 3456–3461, doi: 10.1002/adma.201301244 (2013).
44. Cho, K. *et al.* Gate-bias stress-dependent photoconductive characteristics of multi-layer MoS2 field-effect transistors. *Nanotechnology* **25,** 155201, doi: 10.1088/0957-4484/25/15/155201 (2014).

Acknowledgements

This work was supported by the Ministry of Science and Technology, Taiwan under contract numbers MOST 103–2112-M-001-020-MY3.

Author Contributions

W.-H.W. supervised the project. W.-H.W., F.-Y.S., and Y.-C.W. designed the experiments. Y.-S.S., M.-C.S., and Y.-P.C. performed the STM and STS measurement and analysis. P.-H.H. and C.-W.C. provided the OTS-functionalized substrates. F.-Y.S., Y.-C.W., and T.-S.W. prepared the samples and carried out the photoresponse and transport measurements. F.-Y.S., Y.-C.W., and T.-S.W. analyzed the data. W.-H.W., F.-Y.S., C.-W.C., Y.-F.C. and Y.-P.C. wrote the paper. All authors discussed the results and contributed to the refinement of the paper.

Additional Information

Supplementary information accompanies this paper at http://www.nature.com/srep

Competing Interests: The authors declare no competing financial interests.

How to cite this article: Shih, F.-Y. *et al.* Environment-insensitive and gate-controllable photocurrent enabled by bandgap engineering of MoS_2 junctions. *Sci. Rep.* **7**, 44768; doi: 10.1038/srep44768 (2017).

Publisher's note: Springer Nature remains neutral with regard to jurisdictional claims in published maps and institutional affiliations.